Peroxiredoxin 6 maintains mitochondrial homeostasis and promotes tumor progression through ROS/JNK/p38 MAPK signaling pathway in multiple myeloma

dandan gao
The Second Affiliated Hospital of Xi'an Jiaotong University
Yang Lv
The Second Affiliated Hospital of Xi'an Jiaotong University
Fei Hong
The Second Affiliated Hospital of Xi'an Jiaotong University
Dong Wu
The Second Affiliated Hospital of Xi'an Jiaotong University
Ting Wang
The Second Affiliated Hospital of Xi'an Jiaotong University
Gongzhizi Gao
The Second Affiliated Hospital of Xi'an Jiaotong University
Zujie Lin
The Second Affiliated Hospital of Xi'an Jiaotong University
Ruoyu Yang
The Second Affiliated Hospital of Xi'an Jiaotong University
Jinsong Hu
Xi'an Jiaotong University Health Science Center
Aili He
The Second Affiliated Hospital of Xi'an Jiaotong University
Pengyu Zhang
zhangpengyu2004@126.com

The Second Affiliated Hospital of Xi'an Jiaotong University

Article

Keywords: Multiple myeloma, Apoptosis, Reactive oxygen species, Mitochondrial homeostasis, Bortezomib

Posted Date: March 29th, 2024

DOI: https://doi.org/10.21203/rs.3.rs-4088599/v1

Additional Declarations: No competing interests reported.

Abstract

Peroxiredoxin 6 (PRDX6) is one of the Peroxiredoxin family members with only 1-Cys, using glutathione as the electron donor to reduce peroxides in cells. PRDX6 has been frequently studied and its expression was associated with poor prognosis in many tumors. However, the expression of PRDX6 in multiple myeloma (MM) and its relevance with MM remain unclear. In our study, we found that PRDX6 was overexpressed in MM patients. Its high expression was inversely correlated with prognosis but positively correlated with the levels of β2-microglobulin (B2M), lactate dehydrogenase (LDH), and ISS stage of MM patients. Further, the knockdown of PRDX6 promoted MM cell lines (RPMI 8226, MM.1S, and U266) apoptosis significantly. Mechanically, PRDX6 serves as an anti-oxidative enzyme, and its deficiency led to over-accumulation of reactive oxygen species (ROS), resulting in oxidative stress, following the activation of MAPK signaling pathway, which manifested as phosphorylation of JNK and p38. Then, the expression of BAX and Bcl2 was imbalance, and the cascade cleavage of PARP and caspase3 was increased, ultimately triggering cell apoptosis. In addition, oxidative stress decreased mitochondrial membrane potential (MMP), reduced gene expression levels of oxidative phosphorylation (OXPHOS), and increased in the density of mitochondrial crumpling, leading to mitochondrial structural abnormalities and dysfunction. Furthermore, PRDX6 deficiency combined with bortezomib induced a robust anti-tumor effect in MM cell lines. Finally, in vivo experiments also showed that the knockdown of PRDX6 inhibited tumor growth of tumor-bearing mice. Collectively, PRDX6 protects MM cells from oxidative damage and maintains mitochondrial homeostasis. And targeting PRDX6 is an attractive strategy to enhance the anti-tumor effect of bortezomib in MM.

Introduction

The second most prevalent hematologic malignancy, multiple myeloma (MM), is characterized by uncontrolled expansion of aberrant plasma cells in the bone marrow, which produces an excessive amount of monoclonal immunoglobulin, ultimately leading to hypercalcemia, renal impairment, anemia, or pathologic fracture. Although many novel regiments have been developed to improve MM patients' outcomes over the past decades, the disease is still incurable[1]. Proteasome inhibitors (PIs), particularly bortezomib (BTZ), are one of those that significantly improve the overall survival (OS) of MM patients[2]. Nevertheless, a lot of patients relapsed after receiving initial treatment and developed drug resistance[3]. Thus, it is essential to elucidate the molecular basis of MM pathogenesis and explore effective strategies to enhance the anti-tumor effect of bortezomib in MM.

Peroxiredoxins (PRDXs), the highly conserved family, are sought to be antioxidant enzymes because they can reduce all kinds of peroxide, including hydrogen or lipid peroxides, protecting cells from oxidative damage. There are currently six members of this family, which were divided into two groups: 2-Cys (cysteine) PRDXs and 1-Cys PRDX[4]. The 2-Cys PRDXs, including PRDX1-PRDX5, utilize thioredoxin as the physiological reductant[5]. The sole 1-Cys PRDX (PRDX6) uses glutathione rather than thioredoxin as the electron donor[6]. In addition, PRDX6 is a multifunctional enzyme, which exhibits calcium-independent

phospholipase (iPLA2) activity, lysophosphatidylcholine acyl transferase (LPCAT) activity, and glutathione peroxidase (Gpx) activity[7]. Recent research demonstrated that the expression of PRDX6 is overexpressed in a variety of solid tumors, including lung, ovarian, tongue, and breast cancer[8–11]. Furthermore, some studies revealed that overexpression of PRDX6 in tumors reduces their sensitivity to radiation and chemotherapy, while inhibiting PRDX6 could make tumor cells more sensitive to chemotherapy[12–14]. Although the well-established cytoprotective potential of PRDX6 in solid tumors, its role in MM and the underlying molecular mechanism are unknown.

In this study, we characterized the role of PRDX6 in MM in vitro and in vivo, and illustrated the potential mechanism. We found that PRDX6 was overexpressed in MM patients and its high expression was inversely correlated with OS, but associated with higher lactate dehydrogenase (LDH) and β2-microglobulin (B2M) levels. Knockdown of PRDX6 significantly promoted apoptosis in MM cell lines. Importantly, our research demonstrated that downregulation of PRDX6 promoted bortezomib induced apoptosis, leading to a synergistic anti-tumor effect in MM. Mechanically, PRDX6 deficiency increased apoptosis rate primarily by causing the overaccumulation of reactive oxygen species (ROS), which was then followed by a reduction in mitochondrial membrane potential (MMP) and mitochondrial dysfunction. Finally, we demonstrated that the knockdown of PRDX6 significantly inhibited tumor growth in a tumor-bearing mouse model. In conclusion, our data indicated that PRDX6 is crucial in MM progression, and targeting PRDX6 may be a promising strategy to enhance the anti-tumor effect of bortezomib in MM.

Results

PRDX6 is overexpressed in MM and correlated with poor prognosis

Based on publicly available microarray data from the GEO database, we found the expression of PRDX6 was remarkedly overexpressed in MM patients compared with healthy donors (HD) in GSE6477 (n = 162), GSE47552 (n = 99) and GSE13591 (n = 158) (Fig. 1A-C). To test the association between its expression and overall survival (OS) of MM patients, we evaluated the survival curves in GSE24080 (n = 559) and GSE57317 (n = 55). The curves revealed that PRDX6 expression was negatively correlated with the OS of MM patients (Fig. 1D-E). Subsequently, the relationship between PRDX6 expression and patients' clinical characteristics was assessed in GSE24080. The results showed that PRDX6 expression was positively correlated with the levels of β2-microglobulin (B2M), lactate dehydrogenase (LDH), and ISS stage of MM patients (Table 1). Collectively, these findings indicated that the patients in the PRDX6 high-expression group had poor prognosis and clinical characteristics, suggesting that PRDX6 may have a siginificant role in the onset of MM. Furthermore, we performed receiver operating characteristics (ROC) curves to assess the diagnostic value of PRDX6 in GSE6477. Notably, the area under the curve (AUC) was 0.8259 ($P<0.0001$, 95%CI: 0.7321–0.9197) for HD and newly diagnosed multiple myeloma (NDMM) (Fig. 1F). These figures demonstrated that PRDX6 might function as a biomarker to discriminate HD from different

stages of plasma cell neoplasm, except for monoclonal gammopathy of undetermined significance (MGUS).

Table 1
Clinical characteristics of MM patients according to the expression of PRDX6 in GSE24080 datasets (n = 559)

	Low PRDX6 expression (n = 280)	High PRDX6 expression (n = 279)	t or χ^2/p-value
Gender	163/280 (58.21%)	174/279 (62.37%)	1.006/0.316
Male	117/280 (41.79%)	105/279 (37.63%)	
Female			
Age (year)	56.72 ± 9.89	57.64 ± 9.01	−1.145/0.253
Immunoglobulin subtypes	77/274 (28.10%)	56/265 (21.13%)	4.008/0.405
IgA	154/274 (56.21%)	159/265 (60.00%)	
IgG	1/274 (0.37%)	2/265 (0.76%)	
IgD	39/274 (14.23%)	45/265 (16.98%)	
Light Chain	3/274 (1.09%)	3/265 (1.13%)	
Nonsecretory			
B2M	172	148	4.012/0.045
< 3.5 mg/L	108	131	
≥ 3.5 mg/L			
CRP	171	159	0.972/0.324
< 6 mg/L	107	118	
≥ 6 mg/L			
CREAT (μmol/L)	1.24 ± 1.06	1.41 ± 1.45	−1.611/0.108
ALB	37	40	0.148/0.700
< 3.5 g/L	243	239	
≥ 3.5 g/L			
HGB (g/dL)	11.38 ± 1.81	11.13 ± 1.81	1.605/0.109

MM, multiple myeloma; PRDX6, Peroxiredoxin 6; B2M, β2-Microglobulin; CRP, C-reactive protein; CREAT, Creatinine; ALB, Albumin; HGB, Hemoglobulin; LDH, Lactate dehydrogenase; BMPC, Bone marrow plasma cells; Cyto Abn, Cytogenetic abnormality; ISS, International Staging System. Values of Age, CREAT, HGB, and BMPC are given mean ± SD.

	Low PRDX6 expression (n = 280)	High PRDX6 expression (n = 279)	t or χ^2/p-value
LDH	142	110	7.192/0.007
< 150 U/L	138	169	
≥ 150 U/L			
BMPC (%)	45.51 ± 26.12	47.27 ± 26.45	−0.780/0.436
Cyto Abn	187/280 (66.79%)	165/279 (59.14%)	3.504/0.061
Yes	93/280 (33.21%)	114/279 (50.86%)	
No			
ISS stage	167/268 (62.31%)	144/268 (53.73%)	4.052/0.044
I + II	101/268 (37.69%)	124/268 (46.27%)	
III			
Recurrence	196/280 (70.00%)	195/279 (69.89%)	0.001/0.978
No	84/280 (30.00%)	84/279 (30.11%)	
Yes			

MM, multiple myeloma; PRDX6, Peroxiredoxin 6; B2M, β2-Microglobulin; CRP, C-reactive protein; CREAT, Creatinine; ALB, Albumin; HGB, Hemoglobulin; LDH, Lactate dehydrogenase; BMPC, Bone marrow plasma cells; Cyto Abn, Cytogenetic abnormality; ISS, International Staging System. Values of Age, CREAT, HGB, and BMPC are given mean ± SD.

In the meanwhile, we used qRT-PCR and western blotting to assess the mRNA and protein levels of PRDX6 in BM aspirates from clinical MM patients and different MM cell lines. The results showed that PRDX6 mRNA expression was significantly elevated in MM patients (Fig. 1G-H) and MM cell lines (Fig. 1I) compared with healthy donors. In addition, the protein level of PRDX6 was also markedly upregulated in NDMM and MM cell lines (Fig. 1J). Taken together, these findings suggested that PRDX6 may play an important role in MM development and progression.

Knockdown of PRDX6 promotes apoptosis and inhibits proliferation in vitro

To determine the function of PRDX6 in MM, we conducted the RNA interference strategy to knock down PRDX6 expression in MM cell lines (RPMI 8226, MM.1S, and U266). With specific PRDX6-siRNA, the PRDX6 expression was decreased by 50%-80% in different MM cell lines, as shown by western blotting and qRT-PCR (Fig. 2A-B). Then we performed the CCK-8 assay and found that the knockdown of PRDX6 remarkably decreased cell viability of MM cells (Fig. 2C). Further, we used Annexin V/7-AAD staining to examine whether cell apoptosis could be affected by the knockdown of PRDX6. As a result, after

transfection of MM cells with PRDX6-siRNA, MM cells displayed a significant increase in apoptosis rate (Fig. 2D). Moreover, EdU assay was performed to detect cell proliferation, and we noted that the knockdown of PRDX6 had a small but substantial impact on reducing cell proliferation (Fig. 2E). Next, cell cycle was measured by PI staining, the results showed that PRDX6 knockdown led to cell cycle arrest at the G2/M phase (Fig. 2F). These evidence indicated that PRDX6 may affect the apoptosis, proliferation and cell cycle, which in turn affect the survival and progression of MM.

PRDX6 protects MM cells from oxidative stress and maintains mitochondrial homeostasis

Given the antioxidant effect of PRDX6, we measured the intracellular ROS level after PRDX6 knockdown using DCFH-DA. We noted that compared with the control group, knockdown of PRDX6 significantly increased ROS level by approximately more than 1.5 times in both U266 and MM.1S (Fig. 3A). Excessive ROS suggested that the MM cells were under oxidative stress, which also indicated a possible abnormality in mitochondrial function. Next, we further investigated the mitochondrial membrane potential (MMP) using JC-1 staining. As predicted, we found that after being transfected with PRDX6-siRNA, the MMP declined significantly in both U266 and MM.1S (Fig. 3B). Additionally, oxidative phosphorylation (OXPHOS) is an important process of mitochondrial to produce ATP. To assess this important function of mitochondrial, we examined several OXPHOS genes (NDUFB8, SDHB, UQCRC2, and ATP5A) expression by qRT-PCR. As a result, the knockdown of PRDX6 resulted in remarkably decreased expression of OXPHOS genes in both U266 and MM.1S (Fig. 3C).

Based on the above findings that the knockdown of PRDX6 caused significant apoptosis, we wondered about the effect of PRDX6 knockdown on the Bcl-2 family in MM cells. So we detected the expression of the Bax (proapoptotic) and Bcl2 (antiapoptotic) proteins in U266 and MM.1S. The results showed a significant increase in Bax expression and a significant decrease in Bcl2 expression. In addition, western blotting analyses showed more cleavage of PARP and Caspase 3 caused by knockdown of PRDX6, which revealed the consequent activation of the caspase cascade (Fig. 3D). Then the mitochondria ultrastructure was evaluated by transmission electron microscopy (TEM). We found that significant apoptosis and impaired mitochondrial (cristae were markedly decreased and density was increased) in MM.1S when knockdown of PRDX6 (Fig. 3E). The above data showed that excessive ROS and subsequent oxidative stress led to mitochondrial dysfunction, which ultimately caused irreversible cell apoptosis and death. Therefore, PRDX6 is an important antioxidant enzyme, which could eliminate overaccumulation of ROS and maintain the homeostasis of mitochondrial in MM cells.

Knockdown of PRDX6 improves bortezomib-induced cytotoxicity

As we all know, many drugs have been developed for the treatment of MM, including PIs, immunomodulatory agents, and melphalan. PIs, especially bortezomib, significantly improves MM patients' outcome. Therefore, we wondered whether the anti-tumor activity of bortezomib was altered by

combining the knockdown of PRDX6. To our surprise, there was a significant increase in the apoptosis rate after combined treatment (Fig. 4A). This result revealed that the combination treatment was more dramatically effective than single bortezomib treatment in MM cells. Moreover, we also measured the ROS level and MMP to assess the function of mitochondrial after the combined treatment. The results were, the ROS level was further elevated and the MMP was further reduced when combining bortezomib, compared with single bortezomib treatment (Fig. 4B-C). And there was significant cell death and vacuolated mitochondrial in MM.1S when combined bortezomib with the knockdown of PRDX6 (Fig. 4D). Overall, these data suggested that PRDX6 might be a favorable therapeutic target in MM. It was proved that the administration of bortezomib combined with the knockdown of PRDX6 enhanced cell apoptosis, hence increasing the efficacy of bortezomib alone.

NAC reverses the effect caused by knockdown of PRDX6

To further confirm whether overaccumulation of ROS and mitochondrial dysfunction were responsible for PRDX6 deficiency-induced apoptosis, a ROS scavenger, N-Acetyl-L-cysteine (NAC) was introduced to pretreat MM cells for 1h. And then the MM cells were transfected with PRDX6-siRNA to knock down the expression of PRDX6 or treated with bortezomib. As expected, pretreated with NAC partially reversed the PRDX6 deficiency-, bortezomib-, and combined treatment-mediated apoptosis (Fig. 5A), compared with the respective corresponding control group, which was accompanied with elevated MMP in MM.1S (Fig. 5B), and Supplementary Fig. 1 showed the similar results in U266. In addition, we observed that the expression of Bax and Bcl2 were also reversed by NAC, and the cleaved blot of PARP and Caspase 3 were decreased, compared with knockdown group (Fig. 5C). Pretreated with NAC for 1h, mitochondrial morphology returned normal in MM.1S, compared with knockdown group (Fig. 5D). And the expression of OXPHOS genes were also increased when pretreated with NAC (Fig. 5E).The antioxidant NAC administration blocked uncontrolled ROS overaccumulation, resultant oxidative damage, and mitochondrial dysfunction, suggesting that oxidative stress is responsible for triggering apoptosis and mitochondrial dysfunction by PRDX6 deficiency.

Knockdown of PRDX6 activates JNK/p38 MAPK signal pathway

It was found that oxidative stress caused by excessive accumulation of ROS could regulate the MAPK signaling pathway. Therefore, we examined the proteins in the MAPK signaling pathway when knockdowned PRDX6 and found that the phosphorylation levels of JNK and p38 were elevated, while the total proteins showed no significant changes (Fig. 6A). Subsequently, we introduced p38 inhibitor SB203580 to rescue the effects caused by the knockdown of PRDX6. After PRDX6 knockdown and then treated with SB203580 for 24h, MM cell apoptosis was detected and the results revealed that cell apoptosis was reduced compared to the knockdown group alone (Fig. 6B). Then the MMP was also measured and we found the MMP was increased treated with SB203580, compared to the knockdown group alone (Fig. 6C). Moreover, we observed that the expression of Bax and Bcl2 were also reversed by

SB203580, and the cleaved blot of PARP and Caspase 3 were decreased, compared with knockdown group (Fig. 6D). Finally, we measured the changes in MAPK signaling pathway pretreated with NAC and found that when excess ROS were eliminated with NAC, the phosphorylation levels of JNK and p38 were reduced compared to the knockdown group alone (Fig. 6E). All of the above findings suggest that excess ROS can induce oxidative stress in MM cells and mediate the phosphorylation of JNK and p38 in the MAPK signaling pathway, and that the ROS/JNK/p38 MAPK pathway is a potential mechanism for the apoptosis and mitochondrial dysfunction in MM cells induced by PRDX6 knockdown.

Targeting PRDX6 restrains tumor growth in vivo

To further confirm the role of PRDX6 in vivo, the xenograft tumor animal assay was performed using MM.1S cells stably transfected with PRDX6-shRNA or control vector (Fig. 7A). The result showed that PRDX6 knockdown had a significant effect on inhibiting tumor growth in vivo, compared with the control group (Fig. 7B). And there were significant reductions in the weight and volume of tumor xenografts observed in the knockdown group compared with those in the control groups (Fig. 7C-D). However, there was no change in body weight (Fig. 7E). H&E staining revealed that the tumor cells in the control group were disorganized, with large deep-stained nuclei, multiple nuclei, and reduced cytoplasm, compared with the knockdown group (Fig. 7F). Moreover, the IHC results showed that the proportions of PRDX6-positive, Ki67-positive and Bcl2-positive cells were both decreased in the knockdown group, while Cleaved Caspase 3- and Cleaved PARP-positive cells were increased in the knockdown group (Fig. 7F). These data indicated that targeting PRDX6 might be a promising strategy to restrain MM progression.

Discussion

Multiple myeloma (MM) is one of hematological malignancies, characterized by uncontrolled expansion of clonal and aberrant plasma cells in bone marrow. Due to the rapid tumor growth and drugs treatment, MM cells are inevitably susceptible to oxidative stress, which manifested as the inequality between ROS levels and antioxidant defense systems. Oxidative stress has been also implicated in the pathogenesis of solid tumors and degenerative disorders, including Alzheimer's diseases[15], Parkinson's diseases[16] and cataractogenesis[17]. To cope with the imbalance, tumor cells develop the antioxidant defense systems for their survival and metastasis, which include CAT, SODs, GPX, TRX and PRDXs[18]. These proteins could maintain the intracellular redox state and protect tumor cells from cell death under conditions of oxidative stress[19].

Among them, the PRDXs family is one of the important and highly conserved antioxidant enzymes, which exists in various cellular compartments and can eliminate peroxynitrite, hydrogen peroxide, and organic hydrogen peroxides[20]. Importantly, PRDX6, the only one 1-Cys PRDX, different from classical glutathione peroxidase or other PRDXs, presents additional activities and involves in various cellular signaling pathways[21]. According to recent studies, the upregulation of PRDX6 is found in many different solid tumors and is associated with migration, invasiveness, chemotherapy resistance, and increasing stem

cell properties, especially in NSCLC, colorectal cancer, and esophageal carcinoma[22–24]. Targeting the PRDX6 gene has shown that PRDX6 with GSH peroxidase and acidic iPLA2 activity is essential for cell survival, further demonstrating that PRDX6 expression is vital for survival in tumor cells. Fang et al. demonstrated that PRDX6 promoted Toledo DLBCL cell proliferation via peroxidase activity and PRDX6 knockdown induced Toledo DLBCL cell apoptosis[25]. Moreover, PRDX6 might maintain cell integrity by reducing peroxidation of membrane phospholipids, protecting DNA from damage, and controlling survival signalling during oxidative stress[26].

Although the well-established cytoprotective potential of PRDX6 in solid tumors, there was little information about the role of PRDX6 in MM. Therefore, in our study, we assessed the significance of PRDX6 in MM and we found PRDX6 was upregulated in MM and inversely associated with OS. Furthermore, the knockdown of PRDX6 inhibited cell viability and promoted cell apoptosis via an increased expression of Bax and a decreased expression of Bcl2, accompanied by consequent activation of the caspase cascade (more cleavage of PARP and Caspase 3). The xenograft tumor animal assay also revealed that PRDX6 deficiency inhibited tumor growth. Additionally, bortezomib is the first line of treatment in MM, greatly improving MM patients' outcomes. However, there are many patients who ultimately relapse and become resistant to bortezomib. So, we want to know whether combining PRDX6 deficiency could alter the anti-tumor effect of bortezomib in MM cells. Intriguingly, we noted that the combined treatment induced more apoptotic cells and intense oxidative stress than did bortezomib alone. These data provide novel insight that PRDX6 may be a target for enhancing the efficacy of bortezomib for MM patients.

Mechanically, previous studies reported that PRDX6 could positively regulate oncogenesis and progression by activating the JAK2/STAT3 signalling pathway. Moreover, PRDX6 regulates Erk1/2 phosphorylation, and Erk1/2 activation also promotes PRDX6 gene expression, finally resulting in a positive feedback loop[27,28]. Given that PRDX6 is an antioxidant, we measured intracellular ROS levels, which elevated obviously after the knockdown of PRDX6. These data revealed that PRDX6 deficiency led to over-accumulation of ROS in MM cells. ROS was thought to be the by-product of normal metabolism[29] but was elevated largely when faced with oxidative stress, including hydrogen peroxide (H2O2), hydroxyl radical (·OH), superoxide radical (·O2-), and oxygen (O2). It has been indicated that ROS is an important regulatory factor related to a series of biological phenomena, especially in tumors[30]. Some research has shown that ROS is a common mediator to promote apoptosis. The high level of ROS is deleterious, due to subsequent oxidative stress induces cell apoptosis or necrosis. Thus, intracellular ROS generation and elimination are tightly regulated in tumor cells. In our study, the knockdown of PRDX6 resulted in ROS accumulation and initiated oxidative stress, thus triggering MM cells apoptosis.

MAPK (Mitogen activated protein kinase) is involved in the regulation of cell proliferation, differentiation, transformation, and apoptosis through the phosphorylation of nuclear transcription factors, cytoskeletal proteins, and enzymes, and is closely related to inflammation, tumors, and other diseases.The MAPK signaling pathway includes four protein kinases, including ERK, JNK/SAPK, p38 MAPK, and ERK5/BMK1.

The MAPK signaling pathway has been found to play an important role in the regulation of oxidative stress, inflammation, calcium overload, etc[31]. The MAPK cascade kinase can be activated continuously in response to intracellular ROS accumulation and oxidative stress, mediate the activation of apoptosis initiator Caspase 9 and apoptosis executioner Caspase 3, and regulate the expression of the Bcl2 family of proteins, which are involved in the regulation of the apoptotic cell death process. The Bcl2 family of proteins is regulated, thus participating in the regulation of apoptotic cell death. In our study, we also found that excess ROS can mediate the phosphorylation of JNK and p38 in the MAPK signaling pathway, following the imbalance in the expression of Bax and Bcl2, then the cleavage of PARP and Caspase 3 increased. Therefore, the ROS/JNK/p38 MAPK pathway is a potential mechanism for the apoptosis and mitochondrial dysfunction in MM cells induced by PRDX6 knockdown.

Additionally, excess oxidative stress which broke the balance of redox homeostasis could lead to irreversible damage to cells, such as protein damage, mitochondrial dysfunction[32], a wide range of DNA lesions, and even genomic instability[33]. Mitochondria is an indispensable component in tumor cells, which is essential to tumorigenesis, apoptosis, cancer therapy, and metastasis by orchestrating cellular energy production or transformation and ROS signalling pathway. Studies have reported a tight relationship between PRDX6 and mitochondrial dysfunction, and mitophagy was significantly increased in HepG2 cells after PRDX6 knockout[33]. Phosphorylation of PRDX6 can be targeted to acidic organelles and translocate to damaged mitochondrial membranes[34]. Consistently, our study found the MMP was decreased after the knockdown of PRDX6 in MM cells. Increased JC-1 monomers represented depolarized or inactive mitochondria, which showed up decreased membrane potential and could not effectively eliminate ROS. The depolarized MMP feed-forward promoting ROS production resulted in more serious damage. As an important function of the mitochondrial, OXPHOS is particularly important in the process of producing ATP. To assess this important function of mitochondrial, we checked several OXPHOS genes expression. Knockdown of PRDX6 resulted in remarkably decreased expression of OXPHOS genes, but the specific regulatory mechanism remains to be explored in future work.

Collectively, the knockdown of PRDX6 led to ROS overaccumulation and oxidative stress in MM cells, which resulted in activation of MAPK signal pathway, ultimately mitochondrial dysfunction by decreasing MMP, disturbing the mitochondrial respiration process, and generating more damaged mitochondria. Subsequently, the dysfunctional mitochondria produced more ROS, which eventually aggravated mitochondrial dysfunction. And its knockdown could increase the susceptibility of cells to bortezomib and induce robust apoptosis in MM cells (Fig. 8). Hence, PRDX6 is a crucial enzyme for anti-oxidative response and should be a meaningful biomarker and potential therapeutic target in MM patients. However, there are still some shortcomings, (i) the clinical bone morrow sample sizes of NDMM are too small to properly represent the general facts; (ii) the underlying and complicated mechanism needs to be further explored.

Materials and Methods

Cell lines and cell culture

The human multiple myeloma cell lines were obtained from professor Jinsong Hu of Xi'an Jiaotong University. All these cell lines were identified by STR (Short Tandem Repeat) before the experiments were carried out. Cell lines were grown in RPMI1640 medium (BasalMedium, China) replenished with 10% fetal bovine serum (FBS, Biological Industries, Israel), 100 μg/ml L-glutamine and antibiotics, and incubated in humidified air with 5% CO2 atmosphere at 37°C.

Materials and reagents

The antibodies including rabbit anti-GAPDH (#10494, 1:1000), rabbit anti-PRDX6 (#13585, 1:1000), rabbit anti-Bax (#50599, 1:3000), rabbit anti-Bcl2 (#12789, 1:1000), mouse anti-PARP (#66520, 1:1000), rabbit anti-Caspase 3 (#19677, 1:1000), rabbit anti-JNK (#17572, 1:1000), rabbit anti-p38 (#51115, 1:1000), rabbit anti-Phospho-p38 (#28796, 1:1000) and mouse anti-β-actin (#66009, 1:1000) were bought from Proteintech (USA). Rabbit anti-Phospho-JNK (#4668, 1:1000) was bought from CST (USA). Bortezomib (HY-10227) and p38 MAPK inhibitor SB203580 (HY-10256) were purchased from MedChemExpress (Shanghai, China). N-Acetyl-L-cysteine (A9165) was obtained from Sigma (Sigma-Aldrich, St Louis, MO, USA) and diluted to 5 mM as the final concentration. Puromycin (CAS:58-58-2) was from Solarbio (China).

Cell viability

Cell viability was checked by the Cell Counting Kit-8 assay (CCK-8, 7 sea, Shanghai, China). Cells at the logarithmic growth phase were seeded in 96-well plates at a density of 2×104 cells per well for the indicated times. 24, 48, and 72 h after transfection with PRDX6-siRNA, 10 μl of CCK8 solution was added to each well and the plates continued incubating for 1–4 h at 37°C. Then, Thermo Scientific™ Multiskan™ FC was used to detect the OD values at a wavelength of 450 nm.

Cell apoptosis, cell proliferation, and cell cycle

To measure cell apoptosis, proliferation, and cell cycle, flow cytometry was carried out. Briefly, 1×106 cells per well were seeded in 6-well plates, then exposed to indicated concentrations of bortezomib with/without knockdown of PRDX6 for 24/48 hours. The cell samples were harvested, then stained with 5 μl of 7-amino-actinomycin D (7-AAD, BD Biosciences, San Jose, CA, USA) and 5 μl of Annexin V–fluorescein isothiocyanate (FITC, BD Biosciences) in 50 μl of binding buffer and incubated at 4°C for 15 min. Then, the binding buffer was applied and immediately recorded using a FACS Canto II flow cytometer (BD Biosciences); 10000 events were recorded and analyzed.

Cell cycle was measured by PI staining. Cell samples were fixed with 70% ethanol overnight at 4°C. Then, the cells were incubated with RNase A and PI per the manufacturers' protocol (Beyotime, China). DNA content was then analyzed using a FACS Canto II flow cytometer; 30000 events were recorded and analyzed.

Cell proliferation was measured by EdU assay. Cell samples were fixed with EdU(1x) at 37℃ for 2h. Then, the cells were harvested, fixed for 15min, permeable for 15min as the manufacturers' protocol (Beyotime, China). EdU positive cells were then analyzed using a FACS Canto II flow cytometer; 10000 events were recorded and analyzed. FlowJo 7.6.2 software was used to analyze these data.

Primary MM cells and normal peripheral blood mononuclear cells (PBMCs)

All patients and healthy donors provided written informed consent of using their samples for research purposes. BM aspirates were obtained from patients newly diagnosed with MM and healthy donors. Ficoll-Hipaque density sedimentation was used to isolate PBMCs from blood samples. The study was approved by the ethical committee of Xi'an Jiaotong University (2015 – 186) and performed following relevant named guidelines and regulations. The study was carried out in compliance with the ARRIVE guidelines.

Bioinformatic analysis

Gene expression profiles of GSE6477 (n = 162), GSE47552 (n = 99) and GSE13591 (n = 158) were derived from GEO (https://www.ncbi.nlm.nih.gov/geo/). GEO2R was carried out to analyze the mRNA expression in BM of healthy donors or different stages of plasma cell neoplasm. ROC curve was evaluated based on gene expression in GSE6477. Survival curves were created using the Kaplan-Meier method in patients of GSE24080 (n = 559) and GSE57317 (n = 55), and any differences in the survival curves were compared by the log-rank test.

Transfection of small interfering RNA (siRNA) and short hairpin RNA (shRNA)

MM cells were transiently transfected with siRNA (GenePharma, Shanghai, China) targeting a negative control or PRDX6 at a final concentration of 100 nM using Rfect siRNA/miRNA Transfection Reagent (Baidai biotechnology, China) according to manufacturer's instructions. The sesequences for siRNA of human PRDX6 and negative control was in Supplementary Table 1.

Lentiviral vector containing human PRDX6 shRNA were purchased from Genepharma (Shanghai, China), which was used to knockdown PRDX6 in MM.1S cells. After 48h, transfected cells were treated with 2.5μg/ml puromycin, then the cells were harvested for further animal experimentation.

Transmission electron microscopy

Cells were collected by centrifugation and fixed in 2.5% glutaraldehyde in 0.1 mol/L phosphate buffer (pH 7.4) for 30 min, post fixed in 1% osmium tetraoxide in the same buffer for 30 min, dehydrated in graded ethanol, washed with propylene oxide, embedded in Epon, and then sectioned on an ultramicrotome at 90 nm thickness. Thin

sections were stained with 5% uranyl acetate and 5% lead citrate and then examined on a HITACHI (H-7650) transmission electron microscope at 80 kV.

Assessment of mitochondrial membrane potential (MMP)

The cells underwent the same processing described in 2.4., 24 or 48 h after transfection of PRDX6-siRNA with/without bortezomib, the MMP of cells was evaluated using JC-1 staining (Beyotime, China) following the manufacturer's protocol. By using flow cytometry, we determined 488 nm for JC-1 monomers and 525 nm for JC-1 aggregates, respectively. MMP was measured to compare the ratio of JC-1 monomers/JC-1 aggregates.

Determination of intracellular reactive oxygen species (ROS)

2',7'-dichlorofluorescein diacetate (DCFH-DA, Beyotime, China) staining was used to detect intracellular ROS levels. After transfection of PRDX6-siRNA with/without bortezomib, the cells were harvested and incubated with DCFH-DA (10 μM) for 20 min at 37℃ in the dark, then the ROS levels were measured using flow cytometry.

Quantitative real-time polymerase chain reaction (qRT-PCR)

Total RNA was extracted from treated MM cells using TRIzol reagent (CWBIO, China). RNA concentrations were measured by Nanodrop and reverse-transcribed to cDNA using the cDNA Reverse Transcription Kit (CWBIO, China). qRT-PCR was performed using the SYBR Green PCR kit (CWBIO, China) and the three-step method was applied. Pre-denatured at 95°C for 5 min, denatured at 95°C for 10 s, annealed at 55–60°C for 20 s, and extended at 72°C for 20 s, the last three steps require 40 cycles. The primers are listed. GAPDH was used as control. The $2 - \Delta Ct$ or $2 - \Delta\Delta Ct$ method were used for analysis. The primers were showed in Supplementary Table 2.

Western Blotting

Cells were lysed in lysis buffer and loaded on 12.5% SDS-PAGE gel with equal amounts of proteins, then electro-transferred to PVDF membrane. After blocking for 1.5 h in 5% non-fat dry milk in PBS with Tween 20 (PBST) buffer and incubated with specific primary antibodies overnight at 4℃. After washing with PBST three times, the appropriate secondary antibodies were added. Then incubated at room temperature for 1 h and visualized using the ECL Western Blot Detection kit (Biosharp, China). The pictures were captured with a CCD camera system (MiniChemi610) and analyzed by Image J.

Xenograft tumor mice model

Female BALB/c-Nude mice (3–4 weeks, Gempharmatech, China) were obtained and kept in SPF environment. The mice were randomly divided into control group (n = 5) and knockdown group (n = 5). For subcutaneous xenotransplanted tumor model, 100 μl serum-free RPMI1640 medium containing Matrigel (Corning) (1:1, v/v) and 5×106 cells were injected subcutaneously into flanks of the mice. Then 5×106

MM.1S cells with PRDX6 knockdown were subcutaneously injected per mouse in knockdown group. And 5×106 MM.1S cells with lentivirus-NC were subcutaneously injected per mouse in control group. About 24 days after tumor cell injection, the mice were sacrificed and xenograft tumors were harvested, weighed and processed for immunohistochemistry staining. At the same time, the changes in body weight of mice were recorded every four days. Tumor volume (V = a×b2 / 2; a: the largest superficial diameter, b: the smallest superficial diameter). The study was approved by the ethical committee of Xi'an Jiaotong University (2022 – 1494) and performed following relevant named guidelines and regulations. The study was carried out in compliance with the ARRIVE guidelines.

Immunohistochemistry (IHC) and histological analysis

Paraffin-embedded thin sections (4μm) of tumor tissues were deparaffinized, rehydrated, antigen retrieved, and incubated with primary antibodies overnight at 4℃. Following incubated with secondary antibodies, sections were treated with DAB and hematoxylin prior to visualized with a light microscope (Nikon, Tokyo, Japan). The tumor tissues of mice were also stained with hematoxylin & eosin (H&E) to assess the morphology of tumor cells.

Statistical analysis

Statistical analysis was analyzed by unpaired Student's t-test between two experimental groups. One-way ANOVA was used to compare multiple groups through S-N-K or Dunnett's T3 test and Mann-Whitney U test. Data are presented as mean ± SD as indicated by at least three independent experiments. The GraphPad Prism 9 Software (La Jolla, CA, USA) was used to analyze data. $P < 0.05$ was considered statistically significant.

Authors' contributions

Dandan Gao: Conceptualization, Investigation, Methodology, Software, Validation, Data curation, Formal analysis, Writing–original draft, Visualization. Yang Lv: Methodology, Validation, Data curation, Formal analysis, Investigation, Visualization. Fei Hong: Methodology, Investigation, Visualization. Dong Wu: Software, Validation. Ting Wang: Specimen collection. Gongzhizi Gao: Methodology, Investigation, Visualization. Zujie Lin: Conceptualization, Validation. Ruoyu Yang:Conceptualization, Validation. Jinsong Hu: Methodology. Aili He: Supervision, Writing–review & editing. Pengyu Zhang: Supervision, Writing–review & editing.

Declarations

Authors' contributions

Dandan Gao: Conceptualization, Investigation, Methodology, Software, Validation, Data curation, Formal analysis, Writing–original draft, Visualization. Yang Lv: Methodology, Validation, Data curation, Formal analysis, Investigation, Visualization. Fei Hong: Methodology, Investigation, Visualization. Dong Wu:

Software, Validation. Ting Wang: Specimen collection. Gongzhizi Gao: Methodology, Investigation, Visualization. Zujie Lin: Conceptualization, Validation. Ruoyu Yang:Conceptualization, Validation. Jinsong Hu: Methodology. Aili He: Supervision, Writing–review & editing. Pengyu Zhang: Supervision, Writing–review & editing.

Acknowledgements

We sincerely thank you for the help provided by all lab personnel in this research.

Disclosure statement

No potential conflict of interest was reported by the author(s).

Funding

This work was supported by Natural Science Foundation of Shaanxi Province (Grant Number No. 2022JQ-812).

Data availability statement

All the data generated or analyzed during this study are included in this published article.

Supplementary material

The Supplementary Material for this article can be found in supplementary files.

References

1. Chim CS, Kumar SK, Orlowski RZ, et al. Management of relapsed and refractory multiple myeloma: novel agents, antibodies, immunotherapies and beyond. Leukemia. 2017;32(2):252-262. doi:10.1038/leu.2017.329
2. Gandolfi S, Laubach JP, Hideshima T, Chauhan D, Anderson KC, Richardson PG. The proteasome and proteasome inhibitors in multiple myeloma. Cancer and Metastasis Reviews. 2017;36(4):561-584. doi:10.1007/s10555-017-9707-8
3. Robak P, Drozdz I, Szemraj J, Robak T. Drug resistance in multiple myeloma. Cancer Treatment Reviews. 2018;70:199-208. doi:10.1016/j.ctrv.2018.09.001
4. Rhee SG, Woo HA, Kil IS, Bae SH. Peroxiredoxin Functions as a Peroxidase and a Regulator and Sensor of Local Peroxides. Journal of Biological Chemistry. 2012;287(7):4403-4410. doi:10.1074/jbc.r111.283432
5. Arevalo J, Vázquez-Medina J. The Role of Peroxiredoxin 6 in Cell Signaling. Antioxidants. 2018;7(12):172. doi:10.3390/antiox7120172
6. Zhou S, Lien Y-C, Shuvaeva T, DeBolt K, Feinstein SI, Fisher AB. Functional interaction of glutathione S-transferase pi and peroxiredoxin 6 in intact cells. The International Journal of Biochemistry & Cell

Biology. 2013;45(2):401-407. doi:10.1016/j.biocel.2012.11.005

7. Fisher AB, Dodia C, Sorokina EM, et al. A novel lysophosphatidylcholine acyl transferase activity is expressed by peroxiredoxin 6. Journal of Lipid Research. 2016;57(4):587-596. doi:10.1194/jlr.m064758
8. Yun H-M, Park K-R, Lee HP, et al. PRDX6 promotes lung tumor progression via its GPx and iPLA2 activities. Free Radical Biology and Medicine. 2014;69:367-376. doi:10.1016/j.freeradbiomed.2014.02.001
9. Huang C-F, Sun Z-J, Zhao Y-F, Chen X-M, Jia J, Zhang W-F. Increased expression of peroxiredoxin 6 and cyclophilin A in squamous cell carcinoma of the tongue. Oral Diseases. 2010;17(3):328-334. doi:10.1111/j.1601-0825.2010.01730.x
10. Pak JH, Choi WH, Lee HM, et al. Peroxiredoxin 6 Overexpression Attenuates Cisplatin-Induced Apoptosis in Human Ovarian Cancer Cells. Cancer Investigation. 2010;29(1):21-28. doi:10.3109/07357907.2010.535056
11. Pagaza-Straffon C, Marchat LA, Herrera L, et al. Evaluation of a panel of tumor-associated antigens in breast cancer. Cancer Biomarkers. 2020;27(2):207-211. doi:10.3233/cbm-190708
12. Xu J, Su Q, Gao M, Liang Q, Li J, Chen X. Differential Expression And Effects Of Peroxiredoxin-6 On Drug Resistance And Cancer Stem Cell-Like Properties In Non-Small Cell Lung Cancer. OncoTargets and Therapy. 2019;Volume 12:10477-10486. doi:10.2147/ott.s211125
13. Sahu N, Stephan J-P, Cruz DD, et al. Functional screening implicates miR-371-3p and peroxiredoxin 6 in reversible tolerance to cancer drugs. Nature Communications. 2016;7(1). doi:10.1038/ncomms12351
14. Pak JH, Choi WH, Lee HM, et al. Peroxiredoxin 6 Overexpression Attenuates Cisplatin-Induced Apoptosis in Human Ovarian Cancer Cells. Cancer Investigation. 2010;29(1):21-28. doi:10.3109/07357907.2010.535056
15. Panahzadeh F, Mirnasuri R, Rahmati M. Exercise and Syzygium aromaticum reverse memory deficits, apoptosis and mitochondrial dysfunction of the hippocampus in Alzheimer's disease. Journal of Ethnopharmacology. 2022;286:114871. doi:10.1016/j.jep.2021.114871
16. Mohammadipour A. A focus on natural products for preventing and cure of mitochondrial dysfunction in Parkinson's disease. Metabolic Brain Disease. Published online 2022. doi:10.1007/s11011-022-00931-8
17. Quan Y. Connexin Gap Junctions and Hemichannels in Modulating Lens Redox Homeostasis and Oxidative Stress in Cataractogenesis. Antioxidants (Basel). 2021;2021 Aug 28;10(9):1374.
18. Rhee SG, Chae HZ, Kim K. Peroxiredoxins: A historical overview and speculative preview of novel mechanisms and emerging concepts in cell signaling. Free Radical Biology and Medicine. 2005;38(12):1543-1552. doi:10.1016/j.freeradbiomed.2005.02.026
19. Bannitz-Fernandes R, Aleixo-Silva R, Silva J, et al. Non-Mammalian Prdx6 Enzymes (Proteins with 1-Cys Prdx Mechanism) Display PLA2 Activity Similar to the Human Orthologue. Antioxidants. 2019;8(3):52. doi:10.3390/antiox8030052

20. Fatma N, Kubo E, Sen M, et al. Peroxiredoxin 6 delivery attenuates TNF-α-and glutamate-induced retinal ganglion cell death by limiting ROS levels and maintaining Ca2+ homeostasis. Brain Research. 2008;1233:63-78. doi:10.1016/j.brainres.2008.07.076
21. Arevalo J, Vázquez-Medina J. The Role of Peroxiredoxin 6 in Cell Signaling. Antioxidants. 2018;7(12):172. doi:10.3390/antiox7120172
22. Huang W-S. Expression of PRDX6 Correlates with Migration and Invasiveness of Colorectal Cancer Cells. Cell Physiol Biochem. Published online 2018. doi:10.1159/000495934
23. Xu J, Su Q, Gao M, Liang Q, Li J, Chen X. Differential Expression And Effects Of Peroxiredoxin-6 On Drug Resistance And Cancer Stem Cell-Like Properties In Non-Small Cell Lung Cancer. OncoTargets and Therapy. 2019;Volume 12:10477-10486. doi:10.2147/ott.s211125
24. He Y, Xu W, Xiao Y, et al. Overexpression of Peroxiredoxin 6 (PRDX6) Promotes the Aggressive Phenotypes of Esophageal Squamous Cell Carcinoma. Journal of Cancer. 2018;9(21):3939-3949. doi:10.7150/jca.26041
25. Fang Z, Liu T, Liu X, et al. PRDX6 promotes proliferation and induces chemo-resistance via peroxidase activity in Toledo diffuse large B-cell lymphoma cells. Transl Cancer Res. 2019;8(5):1772-1781. doi:10.21037/tcr.2019.08.36
26. Manevich Y, Shuvaeva T, Dodia C, Kazi A, Feinstein SI, Fisher AB. Binding of peroxiredoxin 6 to substrate determines differential phospholipid hydroperoxide peroxidase and phospholipase A2 activities. Archives of Biochemistry and Biophysics. 2009;485(2):139-149. doi:10.1016/j.abb.2009.02.008
27. Yun H-M, Park K-R, Park MH, et al. PRDX6 promotes tumor development via the JAK2/STAT3 pathway in a urethane-induced lung tumor model. Free Radical Biology and Medicine. 2015;80:136-144. doi:10.1016/j.freeradbiomed.2014.12.022
28. Zha X, Wu G, Zhao X, et al. PRDX6 Protects ARPE-19 Cells from Oxidative Damage via PI3K/AKT Signaling. Cellular Physiology and Biochemistry. 2015;36(6):2217-2228. doi:10.1159/000430186
29. Reczek CR, Chandel NS. ROS-dependent signal transduction. Current Opinion in Cell Biology. 2015;33:8-13. doi:10.1016/j.ceb.2014.09.010
30. Holmström KM, Finkel T. Cellular mechanisms and physiological consequences of redox-dependent signalling. Nature Reviews Molecular Cell Biology. 2014;15(6):411-421. doi:10.1038/nrm3801
31. SOROKINA E M, FEINSTEIN S I, ZHOU S, et al. Intracellular targeting of peroxiredoxin 6 to lysosomal organelles requires MAPK activity and binding to 14-3-3ε [J]. Am J Physiol Cell Physiol, 2011, 300(6): C1430-41.
32. Basel-Vanagaite L, Dallapiccola B, Ramirez-Solis R, et al. Deficiency for the Ubiquitin Ligase UBE3B in a Blepharophimosis-Ptosis-Intellectual-Disability Syndrome. The American Journal of Human Genetics. 2012;91(6):998-1010. doi:10.1016/j.ajhg.2012.10.011
33. Kim TH, Song J, Kim S-H, et al. Piperlongumine treatment inactivates peroxiredoxin 4, exacerbates endoplasmic reticulum stress, and preferentially kills high-grade glioma cells. Neuro-Oncology. 2014;16(10):1354-1364. doi:10.1093/neuonc/nou088

34. López-Grueso MJ, Lagal DJ, García-Jiménez ÁF, et al. Knockout of PRDX6 induces mitochondrial dysfunction and cell cycle arrest at G2/M in HepG2 hepatocarcinoma cells. Redox Biology. 2020;37:101737. doi:10.1016/j.redox.2020.101737

Figures

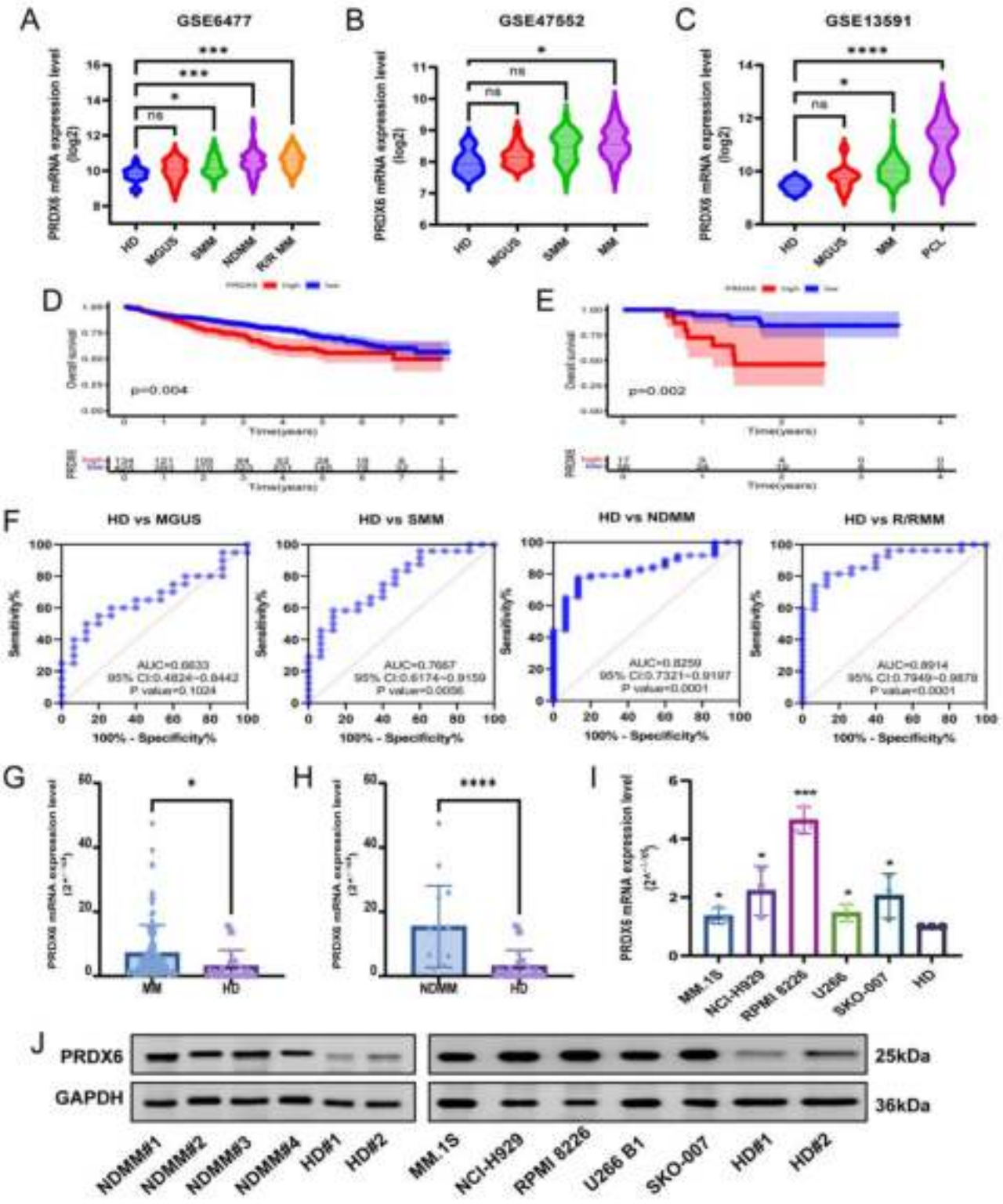

Figure 1

PRDX6 is overexpressed in MM and correlated with poor prognosis of MM patients. (A-C) Analysis of PRDX6 mRNA expression in BM of patients with different stages of plasma cell neoplasm or healthy donors in GSE6477 (n=162) (HD, healthy donors, n=15; MGUS, monoclonal gammopathy of undetermined significance, n=22; SMM, smoldering multiple myeloma, n=24; NDMM, newly diagnosed multiple myeloma, n=73; R/RMM, relapsed or refractory multiple myeloma, n=28), GSE47552 (n=99) (HD, n=5; MGUS, n=20; SMM, n=33; MM, n=741), GSE13591 (n=158) (HD, n=5; MGUS, n=11; MM, n=133; PCL, n=9). (D-E) Kaplan-Meier (KM) survival analysis of PRDX6 in GSE24080 (n=559) (D) and GSE57317 (n=55) (E). (F) ROC curves of PRDX6 in different stages of plasma cell neoplasm in GSE6477. The AUC and p-value were calculated. (G) Analysis of PRDX6 mRNA expression in MM patients (n=84) and HD (n=29) by qRT-PCR. (H) Analysis of PRDX6 mRNA expression in NDMM patients (n=15) and HD (n=29) by qRT-PCR. (I) Analysis of PRDX6 mRNA expression in different MM cell lines and HD by qRT-PCR. (J) Analysis of PRDX6 protein expression in NDMM patients (n=4) and MM cell lines compared with HD (n=2) by Western blotting. The data are the mean ± SD. *p < 0.05, ***p < 0.001, ****p < 0.0001, ns: no significance.

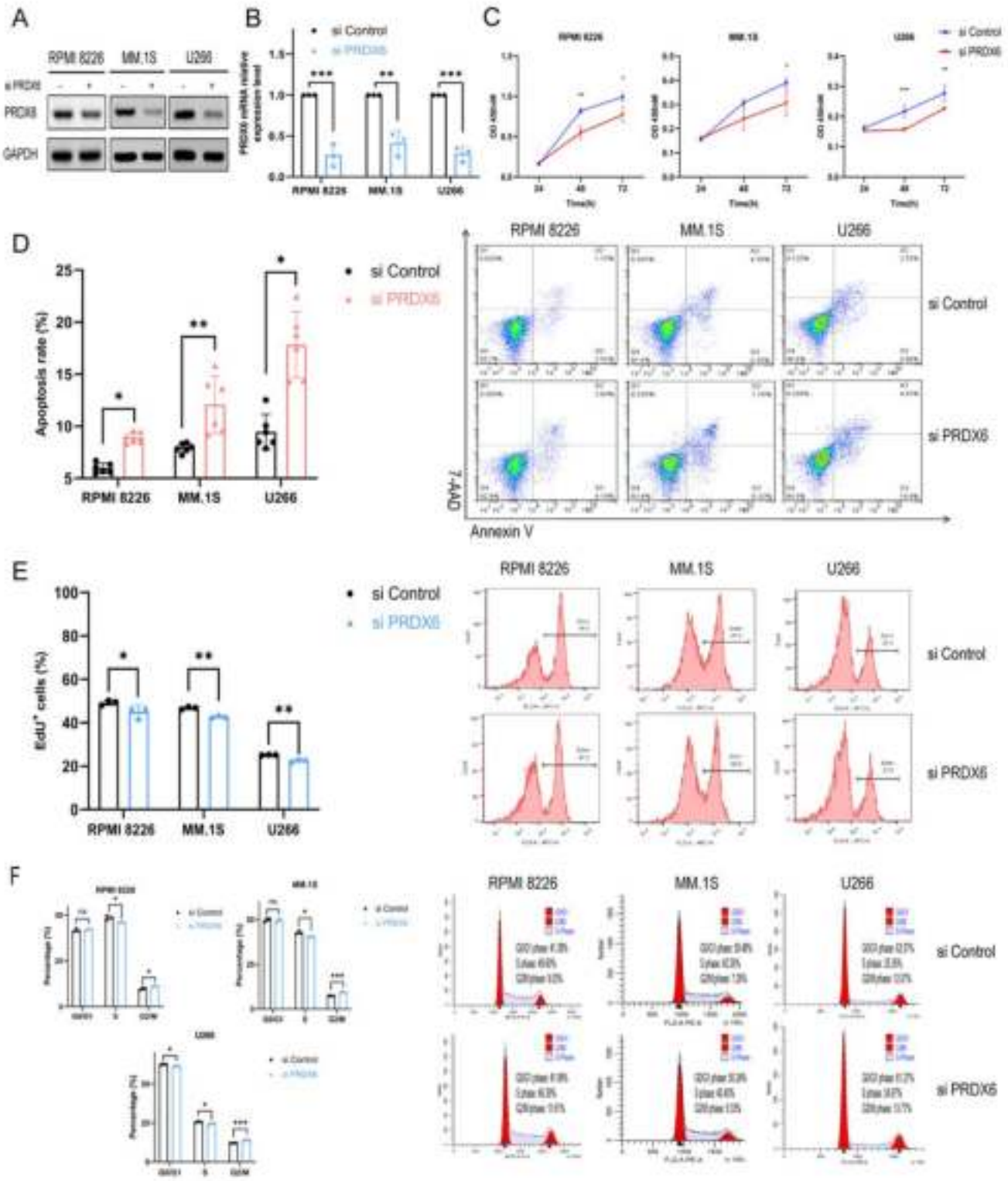

Figure 2

Knockdown of PRDX6 promotes apoptosis and inhibits proliferation in vitro. (A-B) The efficiency of transfection and knockdown was assessed by western blotting and qRT-PCR. (C) Cell viability was detected after knockdown using the CCK-8 assay. (D) Cell apoptosis was detected after knockdown using the Annexin V/7-AAD double staining. (E) Cell proliferation was detected after knockdown using the EdU

staining. (F) Cell cycle was detected after knockdown using the PI staining. The data are the mean ± SD. *p < 0.05, **p < 0.01, ***p < 0.001.

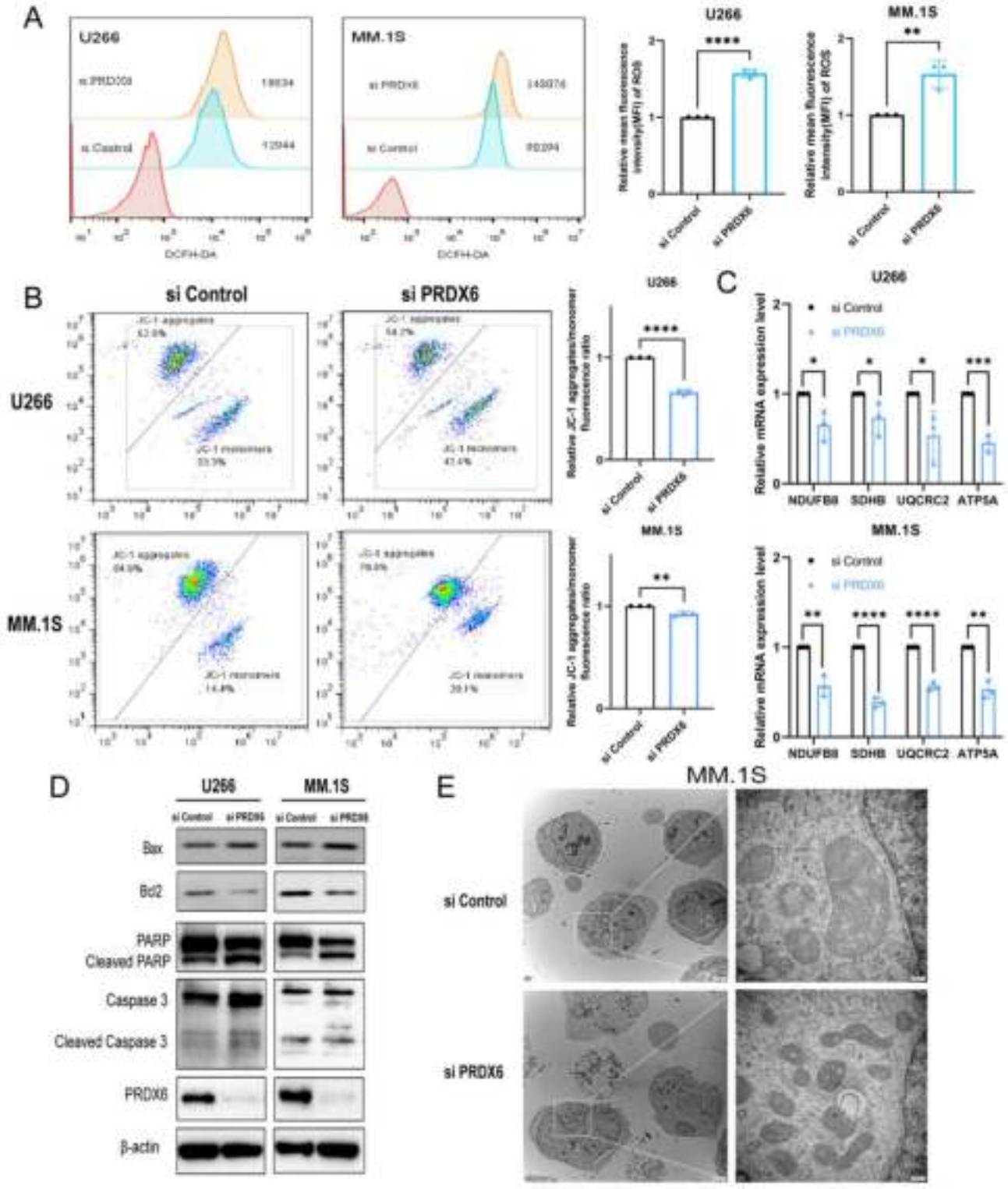

Figure 3

PRDX6 protects MM cells from oxidative stress and maintains mitochondrial homeostasis. (A) ROS was detected using 2',7'-dichlorofluorescein diacetate (DCFH-DA) after the knockdown of PRDX6 in U266 and

MM.1S. (B) Mitochondrial membrane potential (MMP) was measured using the JC-1 Mitochondrial Membrane Potential Assay Kit following the manufacturer's instructions after the knockdown of PRDX6 in U266 and MM.1S. (C) OXPHOS genes mRNA levels were examined by qRT-PCR in U266 and MM.1S. (D) Bax, Bcl2, PARP, Caspase3 and their cleaved blots were detected by western blotting using specific antibodies. (E) Representative images of mitochondria and cell apoptosis in MM.1S visualized by transmission electron microscopy. The data are the mean ± SD. *p < 0.05, **p < 0.01, ***p < 0.001, ****p < 0.0001.

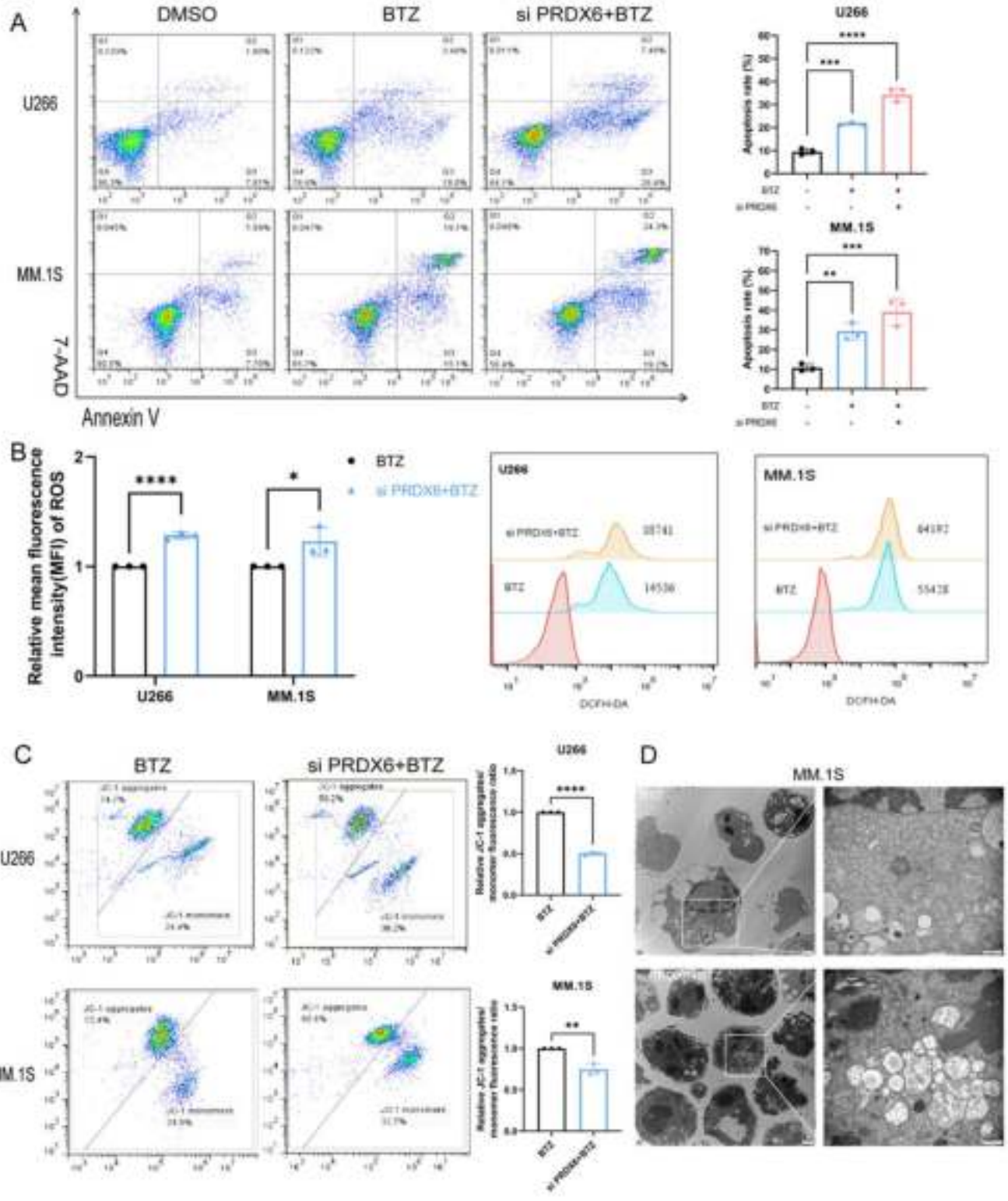

Figure 4

Knockdown of PRDX6 improves bortezomib-induced cytotoxicity. (A) Annexin V/7-AAD double staining was used to detect cell apoptosis when combining knockdown with bortezomib (BTZ) in U266 (BTZ=5nM) and MM.1S (BTZ=50nM). (B) ROS was detected using 2',7'-dichlorofluorescein diacetate (DCFH-DA) when combining knockdown with BTZ in U266 (BTZ=5nM) and MM.1S (BTZ=50nM). (C) Mitochondrial membrane potential (MMP) was measured using the JC-1 Mitochondrial Membrane Potential Assay Kit following the manufacturer's instructions when combining knockdown with BTZ in U266 (BTZ=5nM) and MM.1S (BTZ=50nM). (D) Representative images of mitochondria and cell apoposis in MM.1S visualized by transmission electron microscopy. The data are the mean ± SD. *p < 0.05, **p < 0.01, ***p < 0.001, ****p < 0.0001.

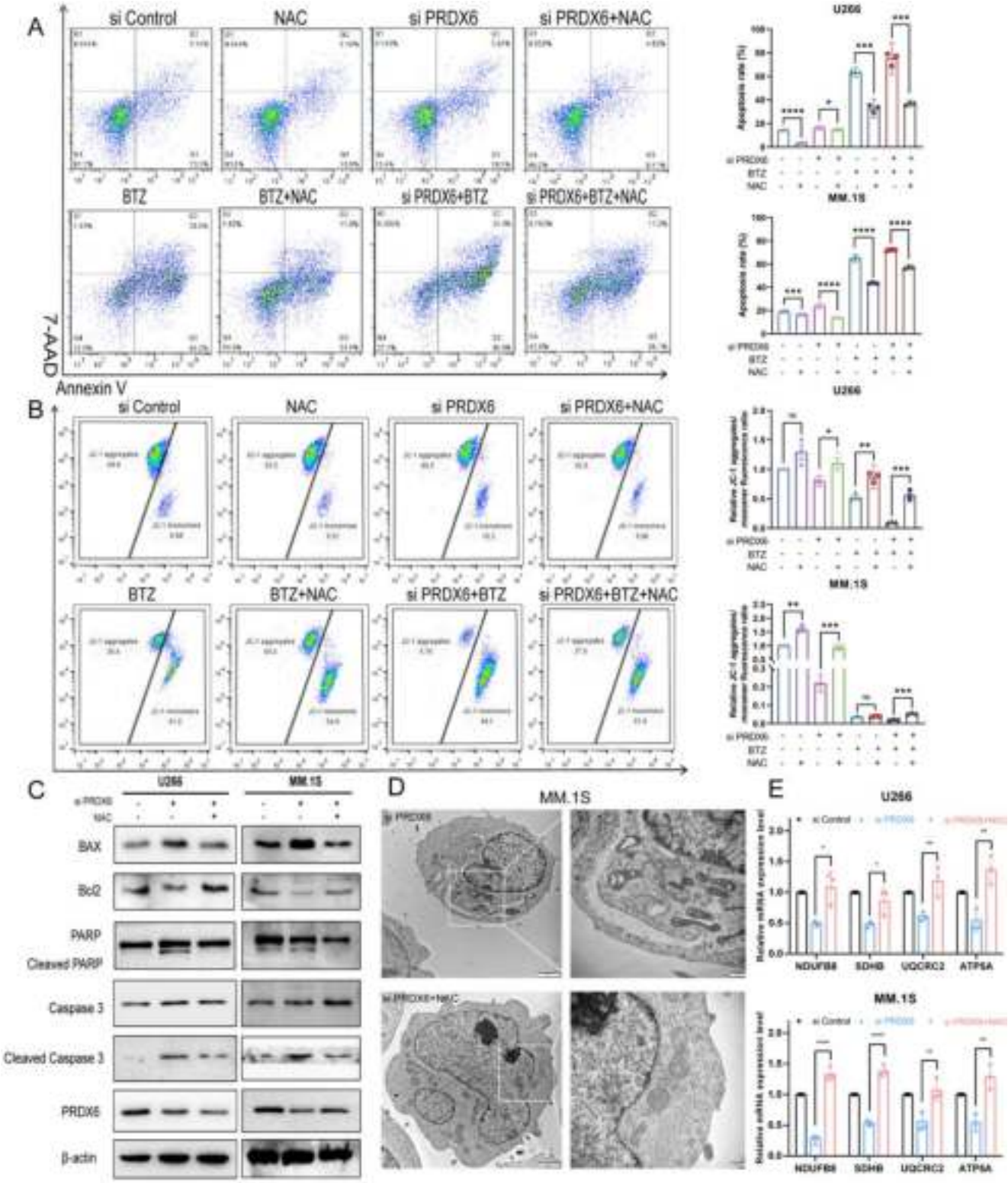

Figure 5

NAC reverses the effect caused by the knockdown of PRDX6. (A-B) After being pretreated with NAC (5 mM) for 1h, the cells were transfected with PRDX6-siRNA with/without bortezomib in MM.1S (BTZ=50nM). Annexin V/7-AAD double staining was used to detect cell apoptosis (A) and JC-1 was used to measure MMP (B). (C) Bax, Bcl2, PARP, Caspase3 and their cleaved blots were detected by western blotting using specific antibodies. (D) Representative images of mitochondria and cell apoposis in

MM.1S visualized by transmission electron microscopy. (E) OXPHOS genes mRNA levels were examined by qRT-PCR in U266 and MM.1S. The data are the mean ± SD. *p < 0.05, **p < 0.01, ***p < 0.001,****p < 0.0001, ns: no significance.

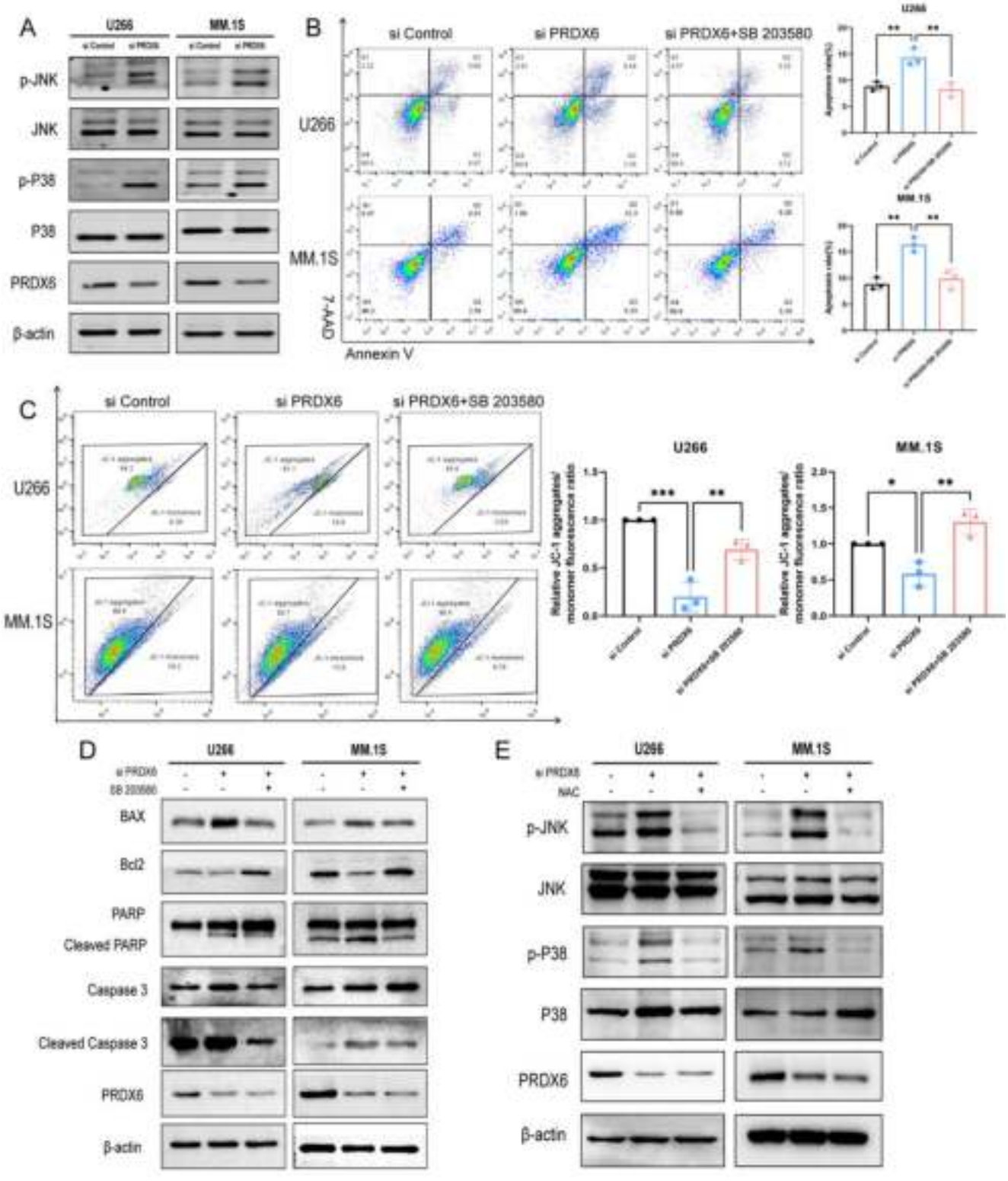

Figure 6

Knockdown of PRDX6 activates JNK/p38 MAPK signal pathway. (A) MAPK signal pathway were detected by western blotting using specific antibodies after knockdown of PRDX6. (B-C) After MM cells were transfected with PRDX6-siRNA, then treated with SB203580 (10 mM) for 24h, Annexin V/7-AAD double staining was used to detect cell apoptosis (B) and JC-1 was used to measure MMP (C). (D) Bax, Bcl2, PARP, Caspase3 and their cleaved blots were detected by western blotting using specific antibodies treated with SB203580 (10 mM) for 24h after knockdown of PRDX6. (E) MAPK signal pathway were detected by western blotting using specific antibodies pretreated with NAC. The data are the mean ± SD. *p < 0.05, **p < 0.01, ***p < 0.001.

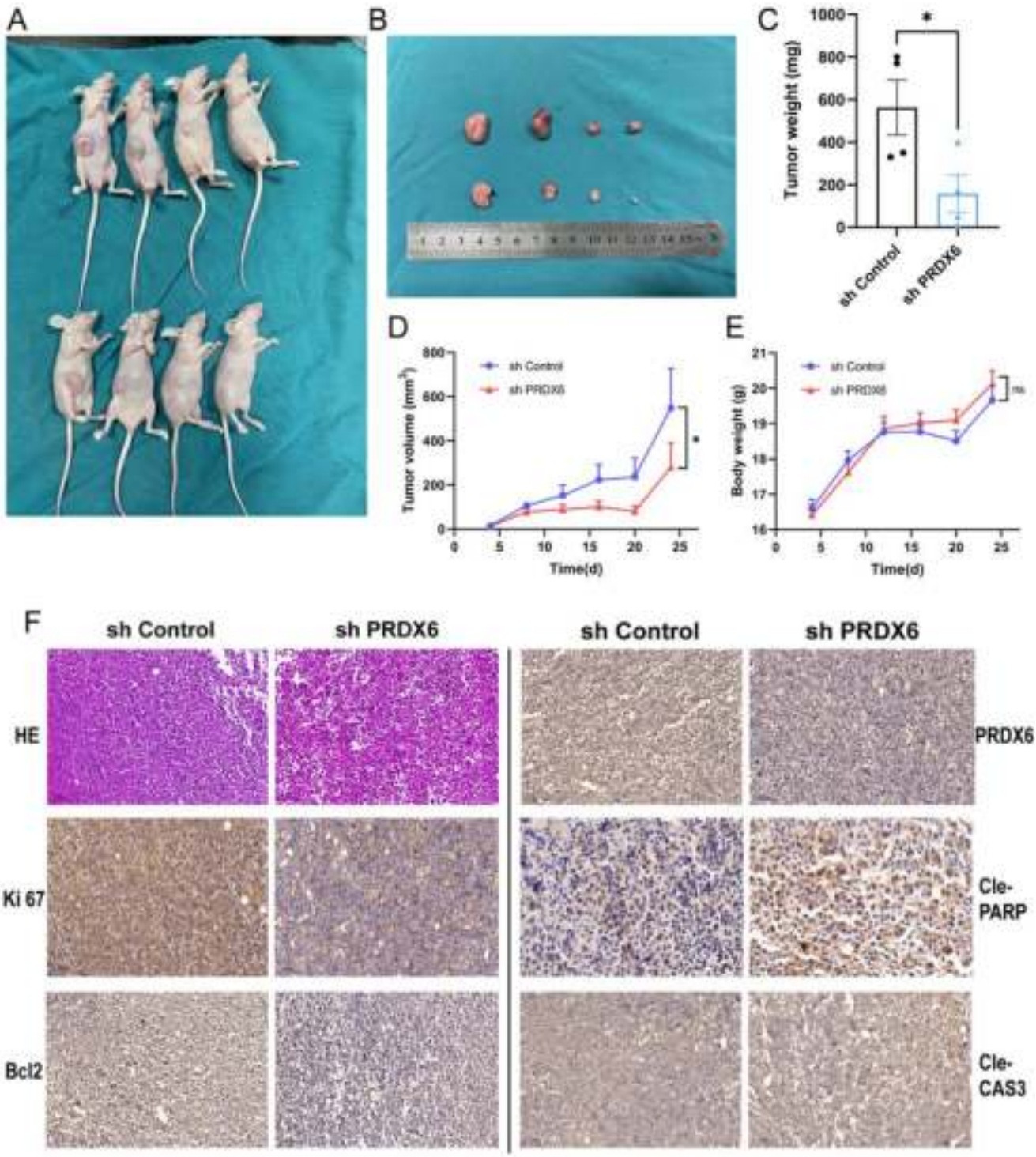

Figure 7

Targeting PRDX6 restrains tumor growth in vivo. (A-B) Representative images of xenograft tumors from MM tumor-bearing mice in the control and knockdown group. (C) Tumor weight of xenograft tumors in the control and knockdown group. (D-E) Growth curves (D) of xenograft tumors and body weight (E) of mice every four days for 24 days. (F) H&E staining and IHC analysis of the protein levels of PRDX6, Ki67,

Bcl2, Cleaved Caspase 3 and Cleaved PARP in tumor tissues from the control and knockdown mice bearing MM xenografts. Scale bar, 100 μm. The data are the mean ± SD. *p < 0.05, ns: no significance.

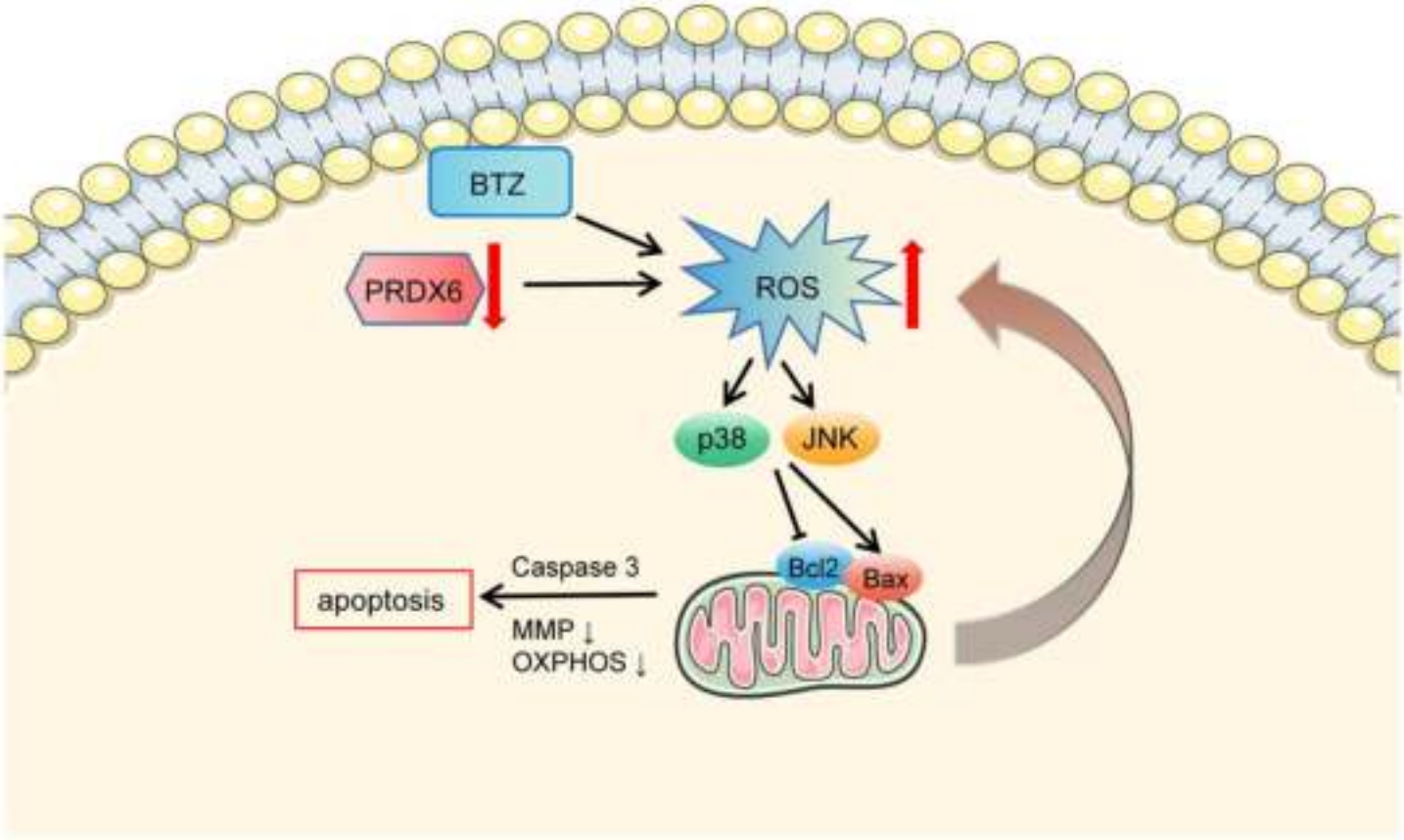

Figure 8

The graphic working model illustrated that PRDX6 deficiency promotes cell apoptosis through overaccumulation of ROS, activation of MAPK signal pathway, decreased MMP, and mitochondrial dysfunction. And PRDX6 deficiency enhanced bortezomib-induced cytotoxicity in MM.

Supplementary Files

This is a list of supplementary files associated with this preprint. Click to download.

- SupplementaryTable1.docx
- SupplementaryTable2.docx
- Supplementaryfigure1.tif